Computational Materials Science 228 (2023) 112312

Contents lists available at ScienceDirect

Computational Materials Science

journal homepage: www.elsevier.com/locate/commatsci

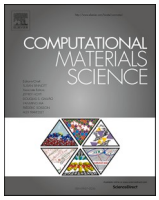

Full Length Article

A potential function of MoS_2 based on machine learning

Lihong Han [a,b], Guoying Qin [a], Baonan Jia [a,b,*], Yingjie Chen [a], Xiaoguang Ma [c], Pengfei Lu [d], Pengfei Guan [e,*]

[a] State Key Laboratory of Information Photonics and Optical Communications, Beijing University of Posts and Telecommunications, Beijing 100876, China
[b] School of Electronic Engineering, Beijing University of Posts and Telecommunications, Beijing 100876, China
[c] Shandong Semiconductor Materials and Optoelectronic Information Technology Innovation Center, Ludong University, Yantai 264025, China
[d] School of Integrated Circuits, Beijing University of Posts and Telecommunications, Beijing 100876, China
[e] Beijing Computational Science Research Center, Beijing 100193, China

ARTICLE INFO

Keywords:
Machine learning
Atomic energy network
Molecular dynamics
Density functional theory

ABSTRACT

MoS_2 has been used as a non-toxic and economical thermoelectric material, which attract the interest of researchers. In terms of computational simulation, system energy is the most basic and important property of microscopic materials. Although the first principles based on density functional theory (DFT) can calculate the energy accurately, the calculation is limited by time and scale. The potential function based on existing data can make up for this shortage. This study uses the Beller-Parrinello (BP) method to construct the machine-learning potential of the Mo-S system. The potential function is trained by the atomic energy network (aenet) software package, and is able to be used in bulk structure and two-dimensional structure. We predicted the energy of structures under different strains and conduct molecular dynamics (MD) simulation to predict the energy change during the simulation process. In addition, we calculated the defect formation energy of MoS_2. The results of ANN were very close to the calculations of DFT. This potential function with high accuracy can greatly shorten the period of exploring the defect structure of MoS_2 and it provides a powerful tool for exploring the large-scale defective MoS_2.

1. Introduction

Monolayer MoS_2 is a member of transition metal dichalcogenide two-dimensional materials, which is a direct bandgap semiconductor with a bandgap of 1.8 eV [1]. It has great potential in the application of optoelectronic devices and has attracted extensive attention from researchers in recent years. The formation energy of MoS_2 can be calculated to explore the stability of different defect states, and the energy barrier during the reaction of MoS_2 can be calculated to explore the transition state. In addition, the calculation of energy is also very important for thermodynamic properties.

In classical physics, the ground state energy is calculated by solving the Schrodinger equation [2]. However, it is complicated to solve Schrodinger equation in a multi-particle system. Density functional theory (DFT) transforms the problem of solving the higher dimensional equation into the problem of solving the charge density function in three dimensions [3–5], which provides an efficient alternative to understand many-particle system. It can calculate the energy of small structures well, so as to calculate various properties. However, the precision of DFT takes the computation time and the computation resource as the cost, and it is difficult to meet the needs of a large system. To make up for the shortage of DFT in the computation cost and calculation scale, it has become a great research craze to fit the potential function through the existing calculation data or experimental data.

In the early research, scholars constructed many empirical potentials [6–9], which are based on the laws of physical interaction and approximate atomic interactions through simple analytical functions. Most empirical potentials have high accuracy for specific structures, which are inexpensive and much faster than first-principles methods. However, the empirical potential is generally specific to a structure and is not flexible. In addition, the fitting of empirical potential is a parametric process, which requires accurate experimental parameters or computational simulation parameters to fit. Liang, Phillpot and Sinnott developed a Mo-S potential and simulated the friction between MoS_2 layers using this potential [10]. Stewart and Spearot improved Mo-S potential to predict the mechanical properties of MoS_2 at athermal

* Corresponding authors.
E-mail addresses: jiabaonan@163.com (B. Jia), pguan@csrc.ac.cn (P. Guan).

https://doi.org/10.1016/j.commatsci.2023.112312
Received 31 October 2022; Received in revised form 2 June 2023; Accepted 3 June 2023
Available online 10 June 2023
0927-0256/

conditions [11]. The Stillinger–Weber (SW) potential describes the two- and three-body interaction that is well applied to thermodynamic property calculation [12]. Although the SW potential has shown advantages in calculating some properties for specific monolayer MoS_2 [13,14], it lacks portability, and has not yet been applied to energy calculation.

Recently, with the development of machine learning technology [15–18], a method of constructing machine learning potential function is proposed to avoid the problem of parameterization. Machine learning potential do not require a prior assumption about the functional form. Local environment descriptors are mapped to potential energy surfaces. The potential function reproduces the first-principle calculation results through the fitting of mathematical expressions. It possesses good transferability, so it has attracted wide attention.

In this paper, the artificial neural network potential function of MoS_2 is constructed by machine learning method, which is suitable for different Mo-S systems. The reliability of the potential function is verified by predicting the energy of bulk MoS_2 and two-dimensional MoS_2. Then we calculate the formation energy of several MoS_2 vacancy defects and further verify the reliability of potential function in defect energy application, which provides favorable conditions for further exploration of MoS_2 defect structure.

2. Computational methodology

2.1. Neural network potential

To construct an accurate MoS_2 potential function, we used the Beller-Parrinello (BP) machine-learning potential method to model the Mo-S system [19,20]. The neural network potential was trained through the atomic energy network (aenet) package, which is provided by Nongnuch Artrith [21,22]. In this method, the system energy is described as the sum of contributions of each atom, and the energy contribution of each atom is obtained by the artificial neural network (ANN) potential function [23,24].

We adopted the network structure of 44–20-20–1, and the structure is shown in Fig. 1. In the network, the number of nodes in hidden layers determines the flexibility of the network and the training time [25]. Through reference adjustment and comparison, we finally chose two hidden layers with 20 nodes. The fourth layer is the output layer, representing the output energy. Data between networks are transmitted through the activation function. Here we chose the Swish activation function [26], which is similar to ReLU activation function [27]. It has

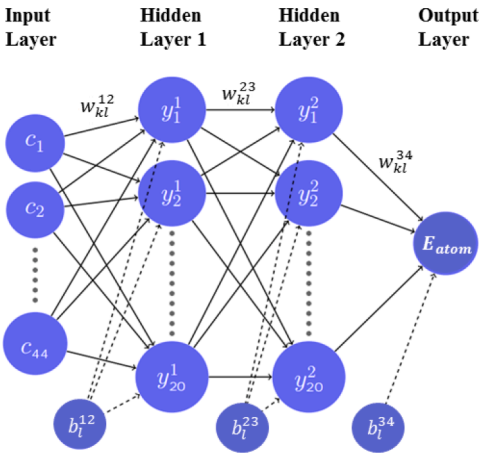

Fig. 1. The four-layer feedforward neural network used in this paper. The network consists of one input layer, two hidden layers, and one output layer with 44 nodes in the input layer, 20 nodes in each of the two hidden layers, and one node in the output layer. The b_l^{ij} represents the bias node, the w_{kl}^{ij} represents the weight, and the arrows represents the direction of transfer.

the advantage that the ReLU function can remove invalid information in training without the problem of training death.

The data set files are partitioned to obtain multiple atomic locales. Each atom locality is divided into 44 components, which are assigned to each node in a vector form. The weight of each node will be adjusted for each training, and the weight of each node will be adjusted many times to make the results converge. By increasing the data set, the weight can be better optimized and the neural network potential prediction results can be more accurate. In the training process, the data multiplicative weight of each node is transferred to the next node (activation function), as shown in Fig. 1.a, taking y_1^1 as an example:

$$y_1^1 = f\left(\sum_{k=1}^{44} c_k w_{k1}^{12} + b_1^{12}\right) \tag{1}$$

Where c_k is the input layer node value, w_{k1}^{12} is the weight,b_1^{12} is the bias node, representing a constant. $f(\,)$ is the activation function.

And so on, the final single atom contribution is expressed as:

$$E_{atom} = f\left(\sum_{k=1}^{20} f\left(y_k^2 w_k\right) + b_3^{34}\right) \tag{2}$$

Where y_k^2 is the value of hidden layer 2, and E_{atom} is the value of output layer that represent the single atom energy.

The energy of the whole structure (E) can be obtained by summing the contributions of all the atoms:

$$E = \sum E_{atom} \tag{3}$$

2.2. Training methods of ANN

To train the accuracy of neural network, we need to build a sufficient number of high-precision data set. We downloaded the existing stable Mo structure, S structure and Mo-S structure from Materials Project [28]. A total of 39 different structures were used for the training process. The space groups of structures contained in the data set are shown in Fig. 2. Here are 6 different structures of Mo crystals, 18 different S crystals and 15 different Mo-S crystals. First, supercell structures with different atomic numbers were obtained by cell expansion, and then all structures were transformed as follows: stretching or compression transformation, increasing shear force, applying strains in three axial directions, applying a perturbation to the structure, and randomly excavating vacancies. In addition, the ab initio molecular dynamics (AIMD) [29] simulations of these structures were performed at temperatures of 300 K.

The energy of the structure was calculated by Vienna ab initio simulation package (VASP) [30,31] based on density functional theory and projection enhanced wave (PAW) [32] method. The generalized gradient approximation (GGA) of the Perdew Burke Ernzerhof (PBE) [33] function was used to exchange the modified functional energy. We set the energy cutoff point of the plane wave basis at 520 eV, and the K-points in the Brillouin zone were automatically generated, while the length was 25. After calculating the energy of the structure, the fingerprint file was used to convert the structure into the '.xsf' file which can be input into the neural network as the data set. We used L-BFGS algorithm to fit the potential function [34], which is a common algorithm in machine learning because of its fast convergence speed and small memory footprint.

There were only a few thousand files in the initial data set. First, we trained the initial potential function, and then observed the distribution of structural energy and predicted results. In the initial training, the structure energy was distributed intermittently, and there were some unstable structures with great prediction deviation. We took the scattered points around the vacancy to conduct AIMD simulation to obtain the structure of the vacancy, and deleted the structure with large errors. Filling in missing values and deleting outliers are often used in machine learning. By filling and deleting data several times, the final data set was closely distributed.

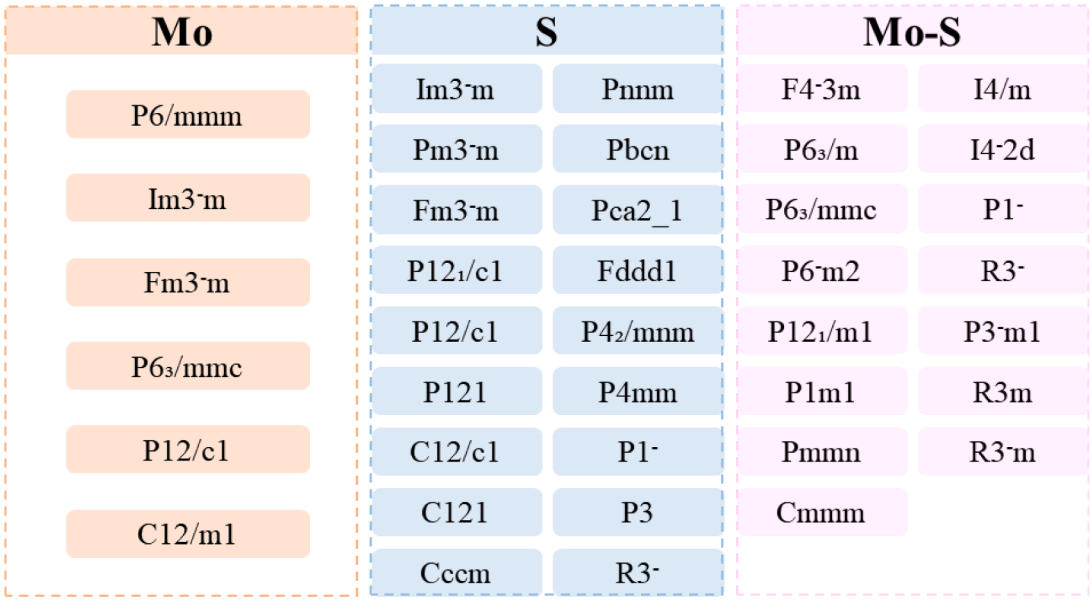

Fig. 2. The 39 different space groups in date set used for the training process.

However, the tight distribution of data set does not mean that the space of data set is perfect. How to make the data set completely cover various atomic local environments still needs to be explored. Therefore, we adopted the 'training-test-supplement' method. We used the existing data set for random segmentation of the training set and the test set, the same batch of data set for 10 times segmentation and training, calculate the root mean square error of each time and take the average. Then we added the new structural data generated by AIMD, re-segment and train the data set, and calculate the root mean square error. When the mean square error obtained after adding the new data is no longer reduced, it indicates that the prediction ability of the potential function previously trained is equal to that of the current training potential function for the test set. Then we think we have a complete data set space. Finally, the training result with the smallest error is taken as the final potential function. This step was time-consuming, but a more reliable means of exploring comprehensive data set.

3. Results and discussion

3.1. The training of potential function

To fit the accurate potential function, we carryed out the 'training-test-supplement' process many times. We finally constructed a data set with 11,187 structures that the ratio of training set to test set was 9:1. In the training set, there are 3651 Mo structures, 2639 S structures and 3779 Mo-S structures. There are 423 Mo structures, 324 S structures and 371 Mo-S structures in the test set. Because there are many stable S structures, configurations with wide energy distribution can be obtained by a small amount of transformation and AIMD simulation, so the final input S elemental structure data into the training set is less than the other two data.

At the beginning of the training, we evaluated the network structure and tested the effect of different network structures with a small number of data sets. We found that the 44–20-20–1 network structure has high accuracy. This network structure was used in the training process. After building a complete data set, we tested different network structures and verified that the network structure with 20 nodes in the two hidden layers has the highest accuracy. The calculation results are shown in Table 1. We find that the network accuracy gradually improved with the increase of the number of nodes from 5 to 20, while the network accuracy drops at 25 nodes. When the number of nodes is small, the network is difficult to reflect the sample correlation and cannot fit the nonlinear output results well, so the error is too large. As the number of nodes increases, the randomness of the training results will also increase, and it is easier to overfit. Finally, it is proved that choosing the 44-20-20-1 network structure is better, and the RMSE is 3.5 meV/atom which is the smallest.

Table 1
Test results of different network structures.

Network configuration	RMSE(meV/atom)
44-5-5-1	16.8
44-10-10-1	5.5
44-15-15-1	4.0
44-20-20-1	3.5
44-25-25-1	5.1

3.2. The test of potential function

We used the trained potential function to draw a comparison chart between DFT results and ANN results of the data set. The abscissa is the average single-atom energy of the structure calculated by DFT, and the ordinate is the average single-atom energy of the structure calculated by ANN. Black stars represent training set data points and red stars represent test set training points. The initial data set was discontinuous and had large error points, as shown in Fig. 3(a). The data points were missing at (−5.5, −4) meV/atom, (−8.8, −8) meV/atom and (−9.7, −9.2) meV/atom. We selected the structures at the edges of these intervals and conducted AIMD simulation on these structures to fill in the missing structures. After completing the missing structure, we selected the sparse points on the diagonal to continue the AIMD simulation to expand the data set. When the error of the test set can no longer be reduced after adding the new data points, we consider that the relatively complete data set is obtained.

By adding more and more data, we finally built a relatively complete data set. As shown in Fig. 3(b), the data points are distributed continuously and closely, with values ranging from −11 to −2.5 meV/atom, indicating that the data set space covers a wide range and is relatively complete. Besides, the data points are basically distributed on the diagonal, indicating that the ANN results are very close to the DFT results, which proves that the training results are very good. In addition, the red

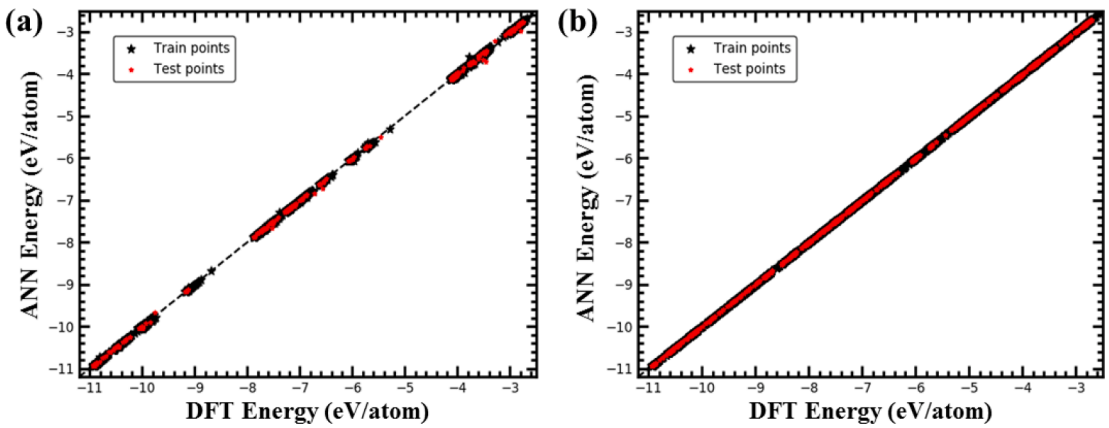

Fig. 3. Energy distribution for all data sets. The abscissa is the DFT calculation result, and the ordinate is the ANN calculation result. The black stars are the training set data, and the red stars are the test set data. (a) Initial data set. (b) Final data set.

test set points almost cover the entire interval and are all on the diagonal, indicating that the potential function can accurately predict any structure in this energy space.

To visually see the error distribution of data sets, we subtracted the DFT calculation results of the data set from the ANN calculation results, and got more than 10,000 data. Then we subtracted minimum error from the maximum error, divided this interval into 13 equally, and counted the data proportion of each interval. As shown in Fig. 4, the median of each interval is rounded as the abscissa, and the data proportion is used as the ordinate to draw the error distribution diagram. It can be seen that about 65% of the data points have errors within 2 meV/atom, and more than 98 % of the data points have errors within 10 meV/atom, indicating that the potential function is very accurate in the data set space. About 18 percent of the data points with errors around −3 meV/atom, and 10 percent of the data points with errors around 4 meV/atom. This potential function is more likely to overestimate the stability of the structure, so that the predicted energy is more likely to be lower than the DFT calculation result.

3.3. Strain test and MD simulation

In order to verify the predictive ability of potential function for structures outside the data set and show that the future potential function can be used in defect state exploration, strain tests and molecular dynamics (MD) simulation were carried out with this potential function [35,36].

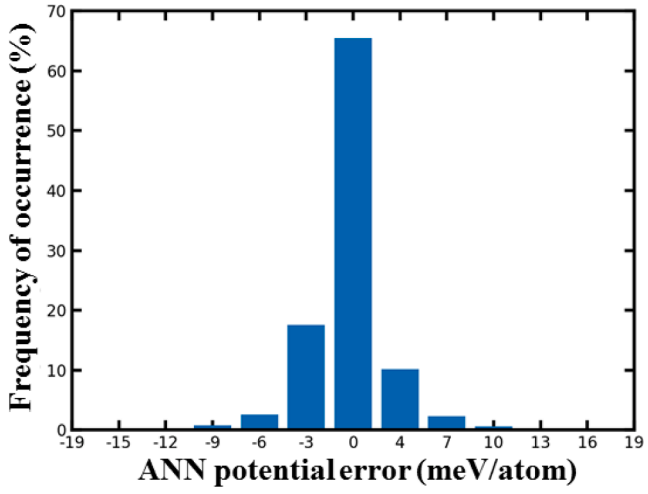

Fig. 4. Bar chart of error distribution of ANN prediction. The abscissa represents the median of the error range (rounded) and the ordinate represents the data proportion.

Different strains were applied to the bulk structure and the two-dimensional structure, and the energy changes of the structure under different strains were calculated using DFT and ANN potential. The SW potential optimized by Jiang et al. [37] is often used to calculate the properties of monolayer MoS_2. We also used SW potential to calculate the energy of two-dimensional structures under different strains. The results are shown in Fig. 5. Not only can ANN predict the structural energy for two-dimensional structures under different strains, but ANN can also predict the bulk structures. For two-dimensional structures, SW can underestimate structural stability, especially under tensile stress. The results of ANN are in good agreement with those of DFT.

We first selected a MoS_2 bulk structure, and the energy of the structure is −21.01 eV when no strain is applied. Then we applied the same strain in all three directions of the structure that from −10 % to 10 %. The negative sign indicating compressive strain and the positive sign indicating tensile strain. As shown in Fig. 5(a), the prediction error increases with the increase of strain. In the compression strains less than 10 %, the prediction errors of ANN are less than 1.9 meV/atom. At 7 % tensile strain, the prediction error of ANN is 2.8 meV/atom. After that, we selected two-dimensional MoS_2 structure with energy of −87.35 eV. In the same way as the bulk structure, the strain test of the two-dimensional structure is carried out. As shown in Fig. 5(b), in the compression strains less than 3 %, the prediction errors of ANN are less than 1.9 meV/atom. At 5 % tensile strain, the prediction error of ANN is 2.0 meV/atom. For two-dimensional structures, the error in energy prediction is larger, but within 2 meV/atom for strains in the −3 % to 5 % range. The errors are less than 19 meV/atom for strains in the −10 % to 8 % range.

The prediction of compressive strain by ANN is better than that by tensile strain, which indicates that the potential function can better describe the interaction between atoms at short distances. When the bond length is too long, the potential function will have a certain deviation.

One of the important uses of potential function is to calculate and predict various properties of materials in combination with MD simulation. Therefore, whether the potential function can be applied to MD simulation is very important. In this paper, we mainly carry out various tests on the structure energy. We used the obtained potential function to conduct MD simulation by Large-scale Atomic/Molecular Massively Parallel Simulator (LAMMPS) [38], and predicted the energy trajectory in the process of MD simulation.

Firstly, we performed MD simulations on the Mo-S bulk structure. The relaxation was performed under the NVT ensemble, the temperature was set at 500 K, and the number of simulation steps was 2000. We intercepted 1000–2000 steps in the simulation process and output a

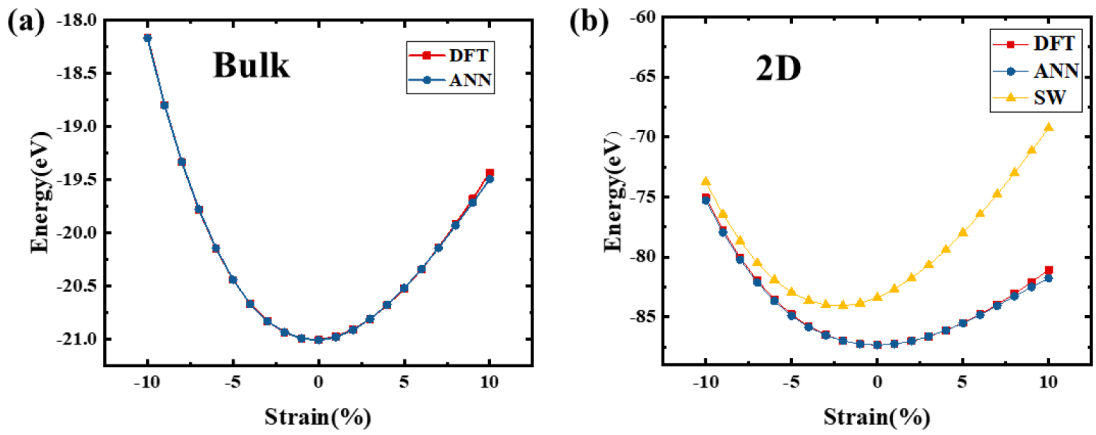

Fig. 5. ANN predicts the change of structural energy under different strains for (a) Mo-S crystal structure and (b) two-dimensional MoS_2 structure. The red dots are the DFT calculation results, the blue dots are the ANN prediction results, and the yellow dots are the SW potential calculation results as a comparison.

structure every 20 steps. The DFT calculation and the ANN prediction were carried out for these structures, and the results of the two methods were compared. As shown in Fig. 6(a), 51 structures were selected for prediction. The prediction errors of 33 structures were less than 5 meV/atom, and that of 47 structures were less than 10 meV/atom. The maximum prediction error of all structures was 16 meV/atom. The DFT calculation result of perfect reproduction of ANN prediction verifies the prediction ability of this potential function for Mo-S bulk structure.

Then we performed the same molecular dynamics simulation on the monolayer MoS_2 structure, and the simulation Settings were the same as the previous Mo-S bulk structure simulation Settings. Similarly, we sampled the structures in the simulation process piecewise, performed DFT calculation and ANN prediction on these structures respectively, and compared the results. As shown in Fig. 6(b), 51 structures were selected for prediction. The prediction errors of 31 structures were less than 5 meV/atom, and that of 48 structures were less than 10 meV/atom. The maximum prediction error of all structures was 12 meV/atom. The predicted results show that the potential function can accurately predict the energy of different structures.

In the process of MD simulation, the structure fluctuates within a certain range, and is not broken. It shows that the setting of potential function is in a reasonable range. In terms of energy prediction, the number of atoms of two-dimensional structure is larger than that of bulk structure, so the deviation of energy prediction is large, but the overall error range is within 12 meV/atom. Therefore, this potential function can be well used in MD simulation.

We expanded the two-dimensional structures used for MD simulation and constructed six structures with different atomic numbers. The energies of structures with atomic numbers of 3, 12, 48, 108 and 192 were calculated using ANN (1 cores with 4 CPU) and DFT (24 cores with 4 CPU), respectively. As shown in Table 2, the largest error of the average single-atom energy between ANN prediction and DFT calculation is 0.83 meV/atom for the structure containing 12 atoms. As the number of atoms increases, the DFT computation time increases rapidly. The structure with 192 atoms takes about 135 min to calculate using DFT, while it only needs 3 s using ANN. ANN can predict structure energy quickly and accurately.

3.4. Prediction of defect formation energy

In order to further verify the application of potential function in the exploration of defective MoS_2, we calculated the defect formation

Table 2
Comparison of calculation time between DFT and ANN.

Atomic number	Energy(eV)		Time(s)	
	DFT	ANN	DFT	ANN
3	−21.84	−21.84	13	<1
12	−87.35	−87.34	115	1
48	−349.38	−349.36	733	1
108	−786.13	−786.06	4467	2
192	−1397.55	−1397.44	8129	3

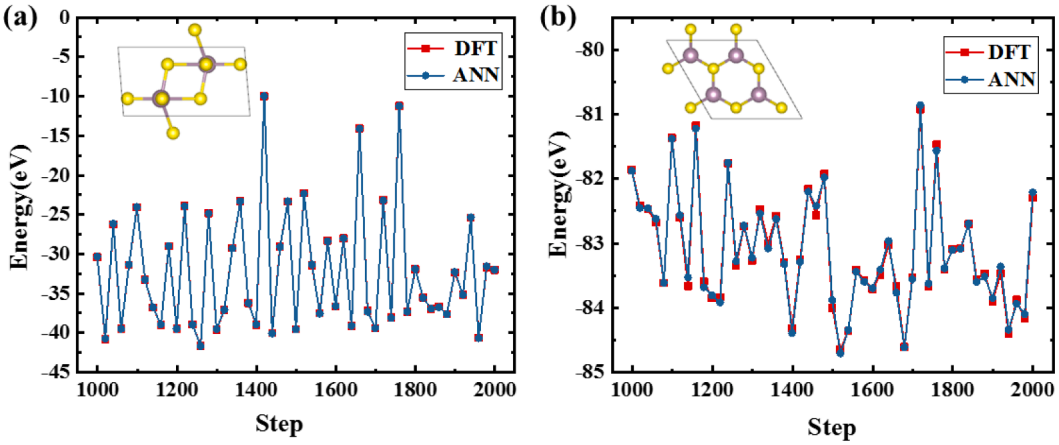

Fig. 6. Energy changes in molecular dynamics simulation trajectories. The red dots are the DFT calculation results, and the blue dots are the ANN prediction results. (a) Energy variation during molecular dynamics simulation of Mo-S crystal structure. (b) Energy variation during molecular dynamics simulation of two-dimensional MoS_2 structure.

energies of different structures with vacancy defect. The defect formation energy is recognized as an important parameter to judge the structural stability and is also the most important property in the study of defect structure. The smaller the defect formation energy, the more stable the corresponding structure will be. The defect formation energy can be obtained by the following equation:

$$E_f = E_t - E_p + \sum_a n_a \mu_a + q(\mu_e + \varepsilon_v) \quad (4)$$

In the equation, E_p represents the total energy of the structure without defects, E_t represents the total energy of the defect structure, and n_a represents the number of atoms a of each element being removed, μ_a is the chemical potential of the corresponding element. The $q(\mu_e + \varepsilon_v)$ represents the effect of electric charge, and we ignored it in the calculation.

We constructed 4 common vacancy defects of MoS_2. The schematic diagram of V_{Mo}, V_S, V_{S2}, and V_{MoS3} are show in Fig. 7. We used DFT and ANN respectively to calculate the defect formation energies of 4 defective structures, and the results are shown in Fig. 8.

For the calculation of defect formation energies of V_{Mo}, V_S, V_{S2}, and V_{MoS3}, the calculation errors of ANN are 0.0159 eV/atom, −0.0087 eV/atom, 0.0032 eV/atom, and −0.0166 eV/atom, respectively. The constructed potential functions show a good ability to predict defect formation energy. It will be used in the exploration of large-scale defective MoS_2.

4. Conclusions

The rapid and accurate calculation of structure energy is helpful to explore defect structure of MoS_2 and promote the study of structural stability of large-scale defective MoS_2. In this work, we constructed the potential function of the Mo-S system by the BP method. By continually adding structures, we constructed a data set space containing 11,187 different structures. Different network structures were tested and the 44–20-20-1 network structure with the highest accuracy was used as the final network structure. We calculated the errors of the data set and plotted the error distribution. More than 98 % of the data points have prediction errors within 10 meV/atom, indicating that our potential function is reliable. We conducted strain tests and MD simulations to further verify the ability of potential function in energy prediction. Our potential function can predict the energy of a structure with a strain of −10 % to 7 % very well, which is far better than the SW potential. The prediction of compressive strain is better than tensile strain, indicating that the potential function can better describe the interaction between

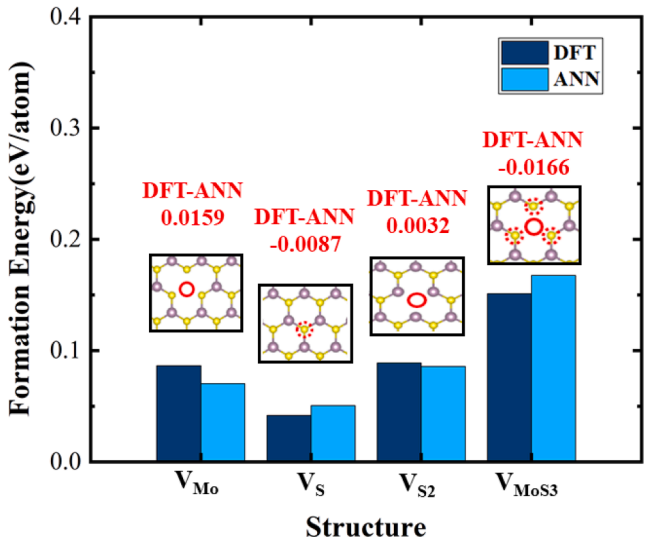

Fig. 8. The defect formation energies calculated by DFT and ANN.

atoms at short distances. The predicted results for energy in the MD simulations further indicate that the potential function can accurately predict the energy of different structures. In addition, ANN is much faster than DFT, which can greatly improve the computational efficiency. We further used this potential function to calculate the defect formation energy and verified the reliability of the potential function in the calculation of defect energy. This work will greatly reduce the energy calculation time for MoS_2 system, and accelerate the exploration of defect states of MoS_2. By the way, the applications of potential functions to mechanical, thermodynamic and electronic properties are being explored.

CRediT authorship contribution statement

Lihong Han: Investigation, Methodology, Writing – original draft, Funding acquisition. **Guoying Qin:** Methodology, Software, Formal analysis, Writing – original draft. **Baonan Jia:** Formal analysis, Data curation, Writing – review & editing. **Yingjie Chen:** Software, Validation, Formal analysis, Data curation. **Xiaoguang Ma:** Investigation, Methodology, Validation. **Pengfei Lu:** Investigation, Methodology, Funding acquisition. **Pengfei Guan:** Investigation, Resources, Supervision, Writing – review & editing.

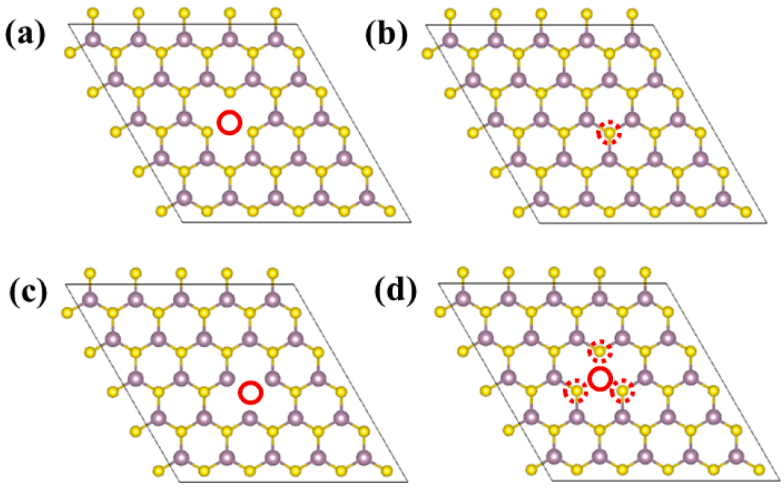

Fig. 7. The schematic diagram of 4 vacancy defects of MoS_2. (a) V_{Mo}. (b) V_S. (c) V_{S2}. (d) V_{MoS3}.

Declaration of Competing Interest

The authors declare that they have no known competing financial interests or personal relationships that could have appeared to influence the work reported in this paper.

Data availability

Data will be made available on request.

Acknowledgments

This study is supported financially by the National Key Research and Development Program of China (No. 2021YFA0718801), the Foundation of Laboratory of Computational Physics (No. 6142A05QN22017), the Project funded by China Postdoctoral Science Foundation (No. 2022M720516), and the Open Project Program of Shandong Semiconductor Materials and Optoelectronic Information Technology Innovation Center, Ludong University. We also acknowledge the computational support from the Beijing Computational Science Research Center (CSRC).

References

[1] J.L. Han, F. Cao, X.H. Ji, Formation mechanism and twist-angle dependent optical properties of bilayer MoS_2 grown by chemical vapor deposition, CrstEngComm 23 (15) (2021) 2889–2896, https://doi.org/10.1039/d0ce01788d.
[2] Z.N. Cai, Y.W. Fan, R. Li, T. Lu, W.Q. Yao, Quantum hydrodynamic model of density functional theory, J. Mathemat. Chem. 51 (7) (2013) 1747–1771, https://doi.org/10.1007/s10910-013-0176-1.
[3] M.K. Nazeeruddin, F. De Angelis, S. Fantacci, A. Selloni, G. Viscardi, P. Liska, S. Ito, T. Bessho, M. Gratzel, Combined experimental and DFT-TDDFT computational study of photoelectrochemical cell ruthenium sensitizers, J. Am. Chem. Soc. 127 (48) (2005) 16835–16847, https://doi.org/10.1021/ja052467l.
[4] M.C. Kim, E. Sim, K. Burke, Understanding and reducing errors in density functional calculations, Phys. Rev. Lett. 111 (7) (2013), 073003, https://doi.org/10.1103/PhysRevLett.111.073003.
[5] P. Geerlings, E. Chamorro, P.K. Chattaraj, F. De Proft, J.L. Gazquez, S.B. Liu, C. Morell, A. Toro-Labbe, A. Vela, P. Ayers, Conceptual density functional theory: status, prospects, issues, Theor. Chem. Acc. 139 (2) (2020) 1–18, https://doi.org/10.1007/s00214-020-2546-7.
[6] A.P. Lima, A.S. Martins, J.S.S. Martins, Lennard-Jones binary fluids: A comparative study between the molecular dynamics and Monte Carlo descriptions of their structural properties, Phys. A 391 (18) (2012) 4281–4289, https://doi.org/10.1016/j.physa.2012.04.003.
[7] A.C.T. van Duin, S. Dasgupta, F. Lorant, W.A. Goddard, ReaxFF: a reactive force field for hydrocarbons, Chem. A Eur. J. 105 (41) (2001) 9396–9409, https://doi.org/10.1021/jp004368u.
[8] Z.H. Shi, J. Zhou, R.J. Li, Application of reaction force field molecular dynamics in lithium batteries, Front. Chem. 8 (2021), 634379, https://doi.org/10.3389/fchem.2020.634379.
[9] T. Liang, Y.K. Shin, Y.T. Cheng, D.E. Yilmaz, K.G. Vishnu, O. Verners, C.Y. Zou, S. R. Phillpot, S.B. Sinnott, A.C.T. van Duin, Reactive potentials for advanced atomistic simulations, Annu. Rev. Mat. Res. 43 (2013) 109–129, https://doi.org/10.1146/annurev-matsci-071312-121610.
[10] T. Liang, S.R. Phillpot, S.B. Sinnott, Parametrization of a reactive many-body potential for Mo–S systems, Phys. Rev. B 79 (24) (2009), 245110, https://doi.org/10.1103/PhysRevB.79.245110.
[11] J.A. Stewart, D.E. Spearot, Atomistic simulations of nanoindentation on the basal plane of crystalline molybdenum disulfide (MoS_2), Model. Simul. Mater. Sci. Eng. 21 (4) (2013), 045003, https://doi.org/10.1088/0965-0393/21/4/045003.
[12] Z.N. Zhang, Y.X. Chen, H. Zheng, A modified Stillinger-Weber potential-based hyperelastic constitutive model for nonlinear elasticity, Int. J. Solids Struct. 51 (7–8) (2014) 1542–1554, https://doi.org/10.1016/j.ijsolstr.2014.01.003.
[13] J.H. Zhao, J.W. Jiang, T. Rabczuk, Temperature-dependent mechanical properties of single-layer molybdenum disulphide: Molecular dynamics nanoindentation simulations, Appl. Phys. Lett. 103 (23) (2013), 231913, https://doi.org/10.1063/1.4844935.
[14] M.L. Li, Y.L. Wan, J.Y. Hu, W.D. Wang, Molecular dynamics simulation of effects of temperature and chirality on the mechanical properties of single-layer molybdenum disulfide, Acta Phys. Sin. 65 (17) (2016), https://doi.org/10.7498/aps.65.176201.
[15] F.V. Prudente, J.J.S. Neto, The fitting of potential energy surfaces using neural networks. Application to the study of the photodissociation processes, Chem. Phys. Lett. 287 (5–6) (1998) 585–589, https://doi.org/10.1016/S0009-2614(98)00207-3.
[16] F.V. Prudente, P.H. Acioli, J.J.S. Neto, The fitting of potential energy surfaces using neural networks: Application to the study of vibrational levels of H-3(+), J. Chem. Phys. 109 (20) (1998) 8801–8808, https://doi.org/10.1063/1.477550.
[17] K.T. No, B.H. Chang, S.Y. Kim, M.S. Jhon, H.A. Scheraga, Description of the potential energy surface of the water dimer with an artificial neural network, Chem. Phys. Lett. 271 (1–3) (1997) 152–156, https://doi.org/10.1016/S0009-2614(97)00448-X.
[18] H.M. Le, H. Sau, L.M. Raff, Molecular dissociation of hydrogen peroxide (HOOH) on a neural network ab initio potential surface with a new configuration sampling method involving gradient fitting, J. Chem. Phys. 131 (1) (2009), 014107, https://doi.org/10.1063/1.3159748.
[19] J. Behler, R. Martonak, D. Donadio, M. Parrinello, Pressure-induced phase transitions in silicon studied by neural network-based metadynamics simulations, Phys. Status Solidi B 245 (12) (2008) 2618–2629, https://doi.org/10.1002/pssb.200844219.
[20] J. Behler, Neural network potential-energy surfaces in chemistry: a tool for large-scale simulations, PCCP 13 (40) (2011) 17930–17955, https://doi.org/10.1039/c1cp21668f.
[21] N. Artrith, A. Urban, G. Ceder, Efficient and accurate machine-learning interpolation of atomic energies in compositions with many species, Phys. Rev. B 96 (1) (2017), 014112, https://doi.org/10.1103/PhysRevB.96.014112.
[22] J. Behler, M. Parrinello, Generalized neural-network representation of high-dimensional potential-energy surfaces, Phys. Rev. Lett. 98 (14) (2007), 146401, https://doi.org/10.1103/PhysRevLett.98.146401.
[23] L.H. Han, X.R. Chen, Q. Wang, Y.J. Chen, M.F. Xu, L.Y. Wu, C.C. Chen, P.F. Lu, P. F. Guan, Neural network potential for studying the thermal conductivity of Sn, Comput. Mater. Sci 200 (2021), 110829, https://doi.org/10.1016/j.commatsci.2021.110829.
[24] N. Artrith, A. Urban, An implementation of artificial neural-network potentials for atomistic materials simulations: Performance for TiO_2, Comput. Mater. Sci 114 (2016) 135–150, https://doi.org/10.1016/j.commatsci.2015.11.047.
[25] J. Schmidt, M.R.G. Marques, S. Botti, M.A.L. Marques, Recent advances and applications of machine learning in solid-state materials science, NPJ Comput. Mater. 5 (2019) 83, https://doi.org/10.1038/s41524-019-0221-0.
[26] Y. Kocak, G.U. Siray, New activation functions for single layer feedforward neural network, Expert Syst. Appl. 164 (2021), 113977, https://doi.org/10.1016/j.eswa.2020.113977.
[27] J. Schmidt-Hieber, Nonparametric regression using deep neural networks with ReLU activation function, Ann. Stat. 48 (4) (2020) 1875–1897, https://doi.org/10.1214/19-AOS1875.
[28] A. Jain, S.P. Ong, G. Hautier, W. Chen, W.D. Richards, S. Dacek, S. Cholia, D. Gunter, D. Skinner, G. Ceder, K.A. Persson, Commentary: The materials project: A materials genome approach to accelerating materials innovation, APL Mater. 1 (1) (2013), 011002, https://doi.org/10.1063/1.4812323.
[29] R. Iftimie, P. Minary, M.E. Tuckerman, Ab initio molecular dynamics: Concepts, recent developments, and future trends, Proc. Nat. Acad. Sci. 102 (19) (2005) 6654–6659, https://doi.org/10.1073/pnas.0500193102.
[30] G. Kresse, J. Furthmuller, Efficient iterative schemes for ab initio total-energy calculations using a plane-wave basis set, Phys. Rev. B 54 (16) (1996) 11169, https://doi.org/10.1103/PhysRevB.54.11169.
[31] G. Kresse, J. Furthmuller, Efficiency of ab-initio total energy calculations for metals and semiconductors using a plane-wave basis set, Comput. Mater. Sci 6 (1) (1996) 15–50, https://doi.org/10.1016/0927-0256(96)00008-0.
[32] P.E. Blochl, Projector augmented-wave method, Phys. Rev. B 50 (24) (1994) 17953, https://doi.org/10.1103/PhysRevB.50.17953.
[33] J.P. Perdew, K. Burke, M. Ernzerhof, Generalized gradient approximation made simple, Phys. Rev. Lett. 77 (18) (1996) 3865, https://doi.org/10.1103/PhysRevLett.78.1396.
[34] A.S. Berahas, M. Takac, A robust multi-batch L-BFGS method for machine learning, Optim. Methods Softw. 35 (1) (2020) 191–219, https://doi.org/10.1080/10556788.2019.1658107.
[35] W. Humphrey, A. Dalke, K. Schulten, VMD: visual molecular dynamics, J. Mol. Graph. 14 (1) (1996) 33–38, https://doi.org/10.1016/0263-7855(96)00018-5.
[36] S. Doerr, M. Majewski, A. Perez, A. Kramer, C. Clementi, F. Noe, T. Giorgino, G. De Fabritiis, TorchMD: A deep learning framework for molecular simulations, J. Chem. Theory Comput. 17 (4) (2021) 2355–2363, https://doi.org/10.1021/acs.jctc.0c01343.
[37] J.W. Jiang, H.S. Park, T. Rabczuk, Molecular dynamics simulations of single-layer molybdenum disulphide (MoS_2): Stillinger-Weber parametrization, mechanical properties, and thermal conductivity, J. Appl. Phys. 114 (6) (2013), 064307, https://doi.org/10.1063/1.4818414.
[38] A. Henry, G. Chen, High thermal conductivity of single polyethylene chains using molecular dynamics simulations, Phys. Rev. Lett. 101 (23) (2008), 235502, https://doi.org/10.1103/PhysRevLett.101.235502.